9`YWffcb]WWcbgYei YbWYg`cZfUbXca `UmYf h\]W_bYgg`Zi Wh]cbg`]b`5`5g#`U5g
gi dYf`Uhh]WYg

Kurt A. Mäder, Lin Wang Wang, and Alex Zunger

Citation:

Electronic consequences of random layer-thickness fluctuations isoelectronic in AlAs/GaAs superlattices

We study the effects of a few types of atomic disorder on the electronic and optical properties of AlAs/GaAs (001) and (111) superlattices: (i) atomic intermixing across the interfaces; (ii) replacing [...] doping); and (iii) random layer-thickness fluctuations in superlattices (SL). Type (i) is an example of lateral disorder, while types (ii) and (iii) are examples of vertical disorder. Using three-dimensional empirical pseudopotential theory and a plane-wave basis, we calculate the band gaps, electronic wave functions, and optical matrix elements for systems containing up to 2000 [...] from the band edges in vertically disordered SLs. Our main findings are: (i) Chemical intermixing across the interface can significantly shift the SL energy levels and even change the identity (e.g., symmetry) of the conduction-band minimum in AlAs/GaAs SLs; (ii) any amount of thickness fluctuations in SLs leads to band-edge wave-function localization; (iii) these fluctuation-induced bound states will emit photons at energies below the "intrinsic" absorption edge (red shift of [...] AlAs/GaAs SLs with monolayer thickness fluctuations have a direct band gap, while the ideal (001) superlattices are indirect for $n < 4$; (vi) there is no mobility edge for vertical transport in a disordered [...] intentionally disordered SLs [A. Sasaki, J. Cryst. Growth 115, 490 (1991)], explaining the strong intensity and large red shift of the photoluminescence in the latter system. We provide predictions for the case of unintentional disorder. © 1995 American Institute of Physics.

I. INTRODUCTION

Experimental and theoretical research on semiconductor superlattices (SL) has, for a long time, focused on ideal, [...] layer thicknesses n and m of the two materials A and G, respectively, while theorists calculated the electronic structure of these ideal structures by applying periodic boundary [...] flicts between experiment (e.g., spectroscopy) and theory (e.g., envelope function $k \cdot p$) are often settled by adjusting some of the theoretical fitting parameters (band offsets, Luttinger parameters, layer thicknesses), thus restoring agreement with experiment. In recent years, attention has shifted somewhat away from ideal to nonideal SLs in two ways: First, with the advent of more sensitive characterization techniques, it has become evident that not only are semiconductor interfaces almost never ideal, but that this unintentional disorder in real samples has discernible spectroscopic and transport consequences[1-10] that should be taken into account by theory. Second, *intentionally* disordered SLs have been proposed[11,12] and grown,[13-15] revealing very interesting disorder-induced effects on the electronic, transport, and optical properties.
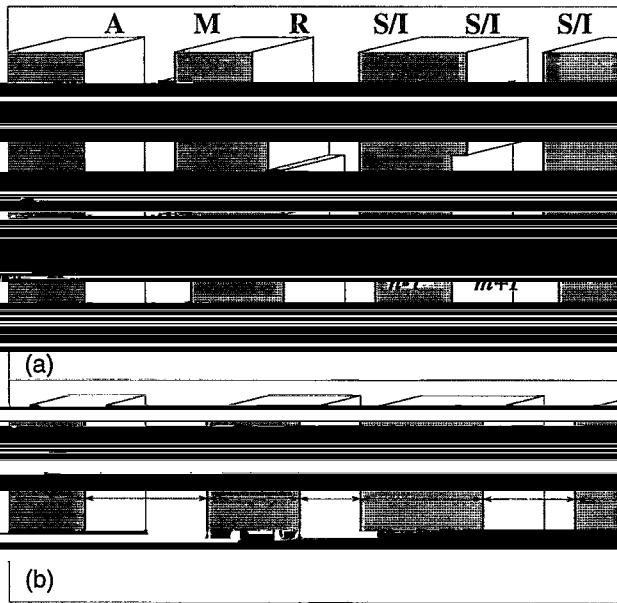
Disorder in a SL can be broadly classified in two catego-

(i)   Lateral disorder in the (x,y) substrate plane[1-5] [Fig. 1(a)], and

(ii)   Vertical disorder along the SL growth direction (z) in the form of discrete layer-thickness fluctuations[6-10] [Fig. 1(b)].

Lateral disorder occurs in the form of chemically intermixed interfaces,[1-3] steps,[4] or islands[5] protruding from material A into G, and vice versa. The translational symmetry of the SL is broken in the (x,y) plane. When averaging over [...] der produces a graded, continuous composition profile along the z axis. Thus, if all of the interfaces in a laterally disordered SL are equivalent, the one-dimensional (1D) periodicity along the growth direction is preserved on average.

Vertical disorder, on the other hand, is characterized by a discrete composition profile along z. Here the interfaces are reasonably flat in the (x,y) plane, but the A and G layer thicknesses fluctuate around their nominal values. The translational symmetry of the SL along z is broken, and the dis-

[a] Present address: Centre Européen de Calcul Atomique et Moléculaire, Ecole Normale Supérieure, 46, Allée d'Italie, 69364 Lyon Cedex 07, France; Electronic mail: mader@cecam.fr

A   M   R   S/I   S/I   S/I

(a)

(b)

tical disorder along the superlattice orientation. The interface structures sketched in cross section in (a) are atomically abrupt (A), "microrough" or

be distinguished in cross section.) In (b) the layer thicknesses fluctuate,

order is "quasi one dimensional" (which does not mean, however, that the Schrödinger equation can be separated into

Unintentional disorder is likely to consist of both types

order depend critically on the coherence length of the experimental probe (x-ray diffraction, electron microscopy, Raman

shown to exhibit a rather complex "roughness spectrum."

scales.[4,18] If the roughness spectrum is bimodal[18] having

large roughness scale, then the probe will "see" an ensemble

in quantum wells of various thicknesses.[7,10,19] If the probe involves excitation of a valence hole or a conduction electron in a cubic semiconductor, its response will predominantly

form of atomic intermixing, the effect on the SL band structure is noticeable predominantly in short-period SLs, but less significant in long-period SLs or multiple quantum wells

If, on the other hand, lateral imperfections consist of large islands, or well-separated steps, the system resembles, in terms of the electronic structure, a SL with vertical thickness

the interfaces labeled "S/I" in Fig. 1(a)].

and great care is taken to assess the effects of any possible

largely concentrated on strictly one-dimensional one-band

mass approximation (EMA), or one-dimensional tight-binding models.[11,25,26] Within 1D models, lateral imperfec-

in the form of mathematically 1D models, if one is willing to ignore the truly 3D crystal structure of a SL. A vast literature exists on localization in 1D disordered systems,[29,30] and

which have been realized experimentally in 3D SLs, e.g., AlAs/GaAs Fibonacci SLs.[13,35,36]

Studies on nonideal SLs using three-dimensional band-

unit cells are required to simulate the absence of periodicity

intermixing in $(AlAs)_1/(GaAs)_1$ (001) SLs has been studied using the local-density approximation (LDA) by considering

layer thicknesses (vertical disorder) and with interfacial

the energy bands is particularly important for short-period

originating from different points in the Brillouin zone. Dis-

erties relative to their ordered counterparts with the same composition:

(a)   strong and initially fast decaying (lifetime $\tau = 0.25$ ns

though the equivalent ordered $(AlAs)_n/(GaAs)_{2}$ SL has an indirect band gap and thus emits both weakly and slowly;

(b) A large red shift ($\sim$60 meV) of the PL peak[44,45] with respect to the equivalent o-SL;

(c) An order-of-magnitude slower rate of reduction of the PL intensity with temperature,[46] and

(d) Nonexponential PL intensity decay at long times[45]

These unusual properties of d-SLs appear very attractive for

on these two types of intentionally disordered SLs has been published in Ref. 47.

(i) The lack of translational symmetry requires the use of unit cells with a macroscopic length $N \approx 1000$ mono-

($Na \approx 300$ nm, where a is the monolayer thickness);

over, occur on a microscopic length scale of about 0.1 nm.

While it is possible to rescale the microscopic length scale by replacing the periodic atomic potential by an external, rectangular potential, this approach fails to describe impor-

microscopic pseudopotential description of the electron structure to a macroscopic length scale necessitated by the absence of translational symmetry. We use fixed (screened)

band structures, effective masses, deformation potentials, band offsets, and energy levels in superlattices.[48] This is also called the empirical pseudopotential method (EPM) in the following. The wave functions are expanded in a basis of

"folded-spectrum" method,[49] where eigenstates are obtained

gap), without having to solve for any of the lower-lying eigenstates first, thus circumventing the need for orthogonal-ization. The effort scales linearly with the number of atoms, allowing us to use the realistic, three-dimensional pseudopo-tentials, and to solve the Schrödinger equation in a highly flexible plane-wave basis even for $N = 1000$ ML. Following these accurate pseudopotential calculations, we also per-formed EMA calculations

(i) to check the validity of the effective mass method, and

(ii) to obtain some statistical properties of the electronic states away from the band edge.

The remainder of the article is organized as follows. In electronic Hamiltonians are discussed in Sec. III. In Sec. IV

SLs are presented. Conclusions and a summary are presented in Sec. V.

II. MODELING THE STRUCTURE OF SUPERLATTICES WITH RANDOM LAYER-THICKNESS FLUCTUATIONS

An ordered, ideal superlattice is characterized by a unit cell A_n/G_m that is repeated periodically, and which contains n monolayers of material A and m monolayers of material

however, instead of the periodic sequence $n,m,n,m,...$ we

[see Fig. 1(b)]. The SL is thus no longer described by the small, $n+m$ atoms unit cell A_n/G_m. Instead, we use a large unit cell that can be described by (normalized) distribution

ing a layer of material $\alpha = A$, or $\alpha = G$ with thickness of n monolayers. We usually require that

however, be easily relaxed by allowing $p_\alpha(0) > 0$. For ex-ample, $p_G(0) > 0$ means "skip a layer of material G" with probability $p_G(0)$.] By requiring the two materials A and G to alternate, one considers in effect the joint distribution function $P(A_n G_m)$ of one-dimensional "molecules" $A_n G_m$,

Sasaki et al.[15] chose this type of random sequence, with $p_A(n) = p_G(n) = p(n)$, for A = AlAs and G = GaAs. These
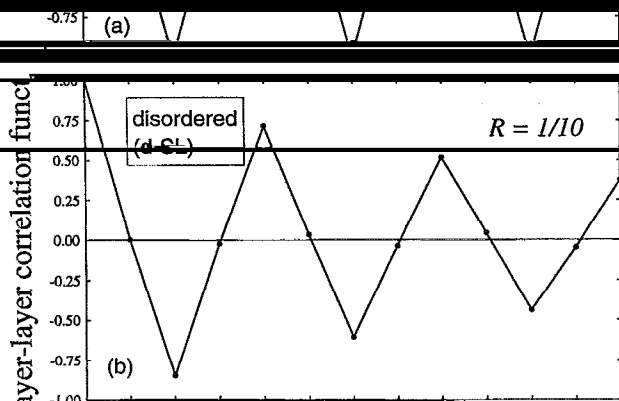
The form of Eq. (1) is also expected in SLs with uninten-tional random thickness fluctuations, if these fluctuations do not depend on the material deposition sequence (i.e., if there are no asymmetries of growing G on A with respect to growing A-on-G).

Modifications of Eq. (1) have also been considered in intentionally disordered SLs. Chomette et al. fixed the thickness of the AlAs segments to a constant n_0, hence, $P(A_n G_m) = p_G(m) \delta(n - n_0)$, (where $n_0 \approx 10$), and $p_G(m)$ was chosen to be a discrete Gaussian distribution around a mean thickness $\langle m \rangle \approx 10$ ML. Arent et al.[45] on the other hand, fixed the length $M = n + m$ of each "molecule" using $P(A_n G_{M-n}) = p(n)$, where the distribution $p(n)$ was chosen to be the same as that used by Sasaki et al.[15] In this approach $p_A(n)$ and $p_G(m)$ are completely correlated, since knowl-edge of one completely specifies the other. Therefore, in con-trast to Sasaki et al.'s d-SL, Arent et al.'s variation corre-sponds to partially ordered SLs (po-SL), retaining long-range order.

SL direction is conveniently measured in terms of the it, one assigns a pseudospin variable S_i of value $+1$ (-1) if

$[p(2) = \frac{5}{6}$ and $p(1) = p(3) = \frac{1}{12}]$, i.e., for a d-SL with average

FIG. 2. Layer–layer correlation function $\langle \Pi_2(j) \rangle$ [Eq. (2)] of (a) an ordered $(A)_2/(G)_2$ superlattice (o-SL), (b) a disordered superlattice (d-SL) with a small degree $R = 1/10$ of thickness fluctuations [Eq. (3)], and (c) a d-SL with maximum disorder $R = 1$.

$$R = \frac{p(n+1)}{p(n)} = \frac{p(n-1)}{p(n)}. \tag{3}$$

Because the distribution $p(n')$ is normalized, we can write $p(n) = 1/(1+2R)$ and $p(n \pm 1) = R/(1+2R)$. For the ideal, ordered $n \times n$ superlattice $R = 0$, and $p(n') = \delta(n' - n)$, whereas for a d-SL with $R = 1$ all three layer thicknesses $\{n-1, n, n+1\}$ occur with equal probability $p = \frac{1}{3}$. The minimum value of R that can be reached in a SL of finite length N corresponds to a single "chain mutation," (a single

monolayer i is occupied by material $A(G)$. The pair-correlation function for two monolayers separated by dis-

where sum runs over the N monolayers of a particular realization of the SL, and the angular brackets denote a configurational average. In an ordered A_n/G_m SL we have in Eq. (2) $N = n + m$ and $\langle \Pi_2(j) \rangle$ is a periodic function with periodicity $n + m$. This is illustrated in Fig. 2(a) for an A_2/G_2 o-SL,

disordered SL, however, we must perform the configurational average in Eq. (2), or equivalently consider the limit

The one-dimensional Fourier transform of the real-space correlation functions of Eq. (2) equals $|S(k_\parallel)|^2$, where $k_\parallel$ is a wave vector along the SL direction. The form factor $|S(k_\parallel)|^2$ is proportional to the diffuse scattering intensity of a kinematic scattering experiment at zero temperature. Figure 3(a) shows $|S(k_\parallel)|^2$ of the ordered SL with correlation function $\langle \Pi_2(j) \rangle$ depicted in Fig. 2(a), for $k_\parallel$ lying in the first Brillouin zone of the empty linear chain. Clearly, the "diffuse scattering" of the o-SL consists of the new Bragg, or satellite peaks

to true diffuse scattering throughout the 1D Brillouin zone. The average periodicity $\langle n \rangle + \langle m \rangle = 4$ still leaves fingerprints at the peak positions of the o-SL. (In the case $R = 1$, there is also a maximum at the previously forbidden wave vector $k_\parallel = \frac{1}{2}$.)

layer correlation function $\langle \Pi_2(j) \rangle$ is periodic, but its amplitude is smaller than that of the ideal o-SL. Figure 4 shows $\langle \Pi_2(j) \rangle$ for po-SLs with $\langle n \rangle = 2$, $R = \frac{1}{10}$, and $R = 1$ exhibiting
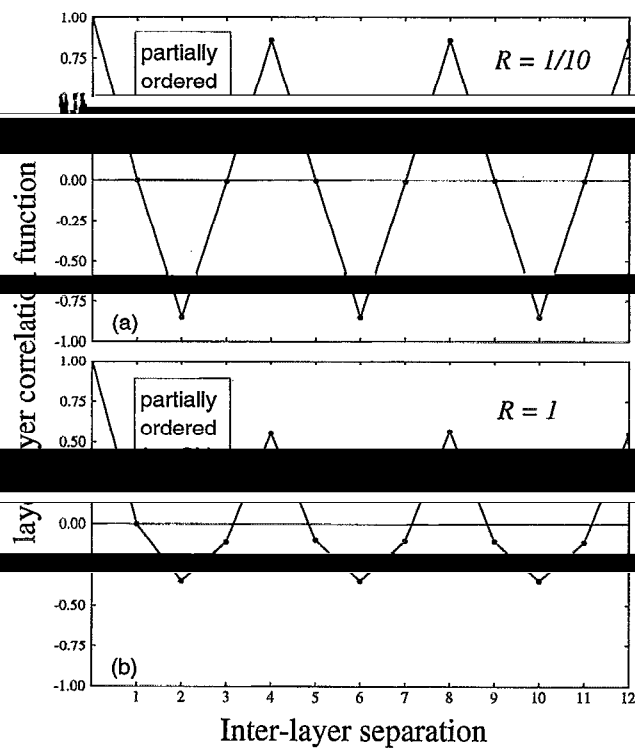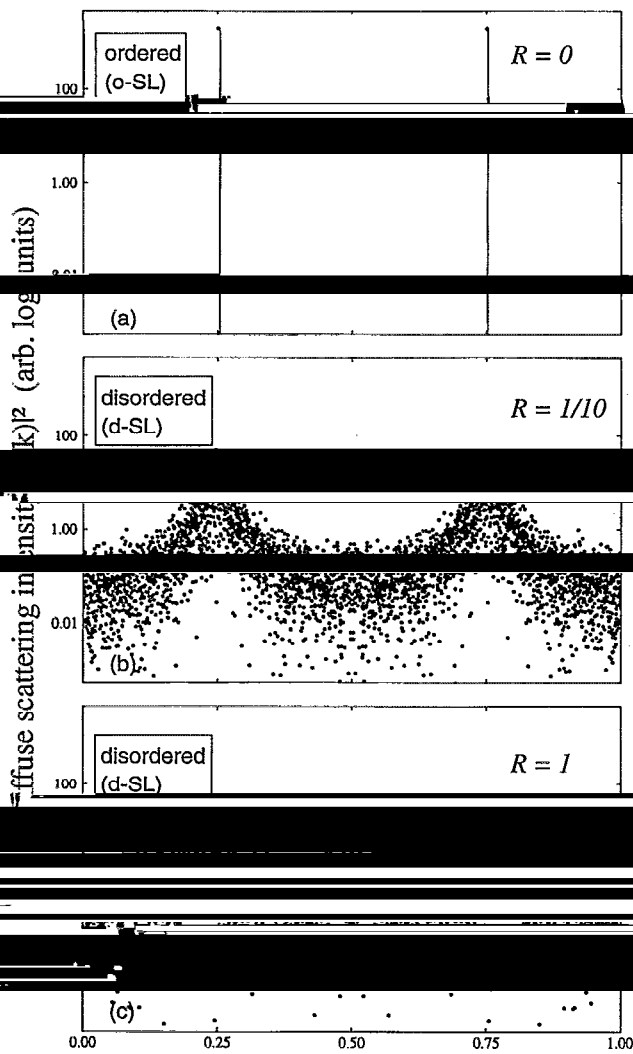
[This article is copyrighted as indicated in the article. Reuse of AIP content is subject to the terms at: http://scitation.aip.org/termsconditions. Downloaded to] IP: 128.138.41.170 On: Tue, 14 Jul 2015 11:52:34

FIG. 3. The diffuse scattering intensities $|S(k_\parallel)|^2$ of the d-SLs shown in Figs. 2(a), 2(b), and 2(c), respectively.

coexistence of rather strong peaks at the o-SL peak positions (marked by vertical impulses) and a diffuse background of comparable amplitude than in a d-SL (Fig. 3).
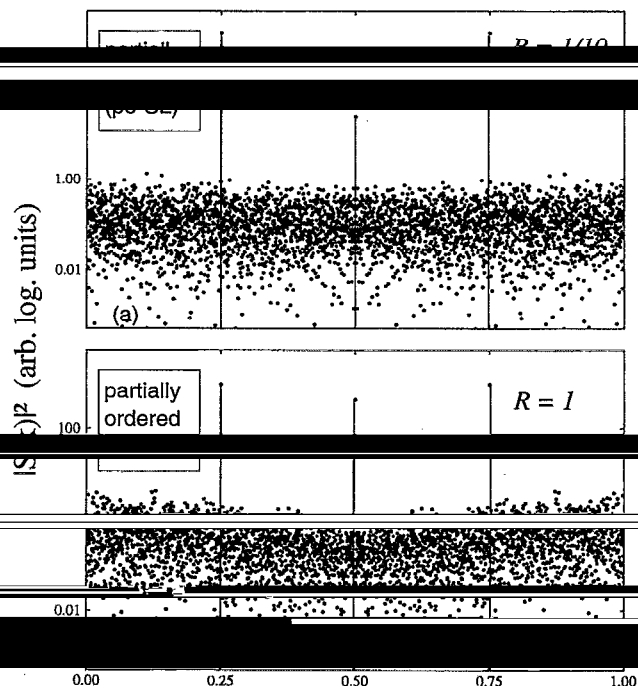
The appearance of diffuse scattering intensity in a d-SL is in fact a manifestation of the relaxation of the $k_\parallel$ selection rule due to the breaking of translational symmetry in the d-SL. We see in the following sections that the relaxation of the $k_\parallel$ selection rule has a profound effect also on the electronic structure of disordered superlattices.

III. ELECTRONIC STRUCTURE CALCULATIONS

A. Three-dimensional pseudopotential representation

1. The pseudopotential and the basis set

Given the crystal structure of an ordered or disordered SL

Figs. 4(a) and 4(b), respectively.

pseudopotential,

$$V(\mathbf{r}) = \sum_\alpha \sum_R v_\alpha(|\mathbf{r} - \boldsymbol{\tau}_\alpha - \mathbf{R}_n|), \qquad (5)$$

cells n of the screened atomic pseudopotentials $v_\alpha(r)$. We have recently parameterized $v_\alpha(r)$ for α=Ga, Al, and As, so

$(\mathrm{GaAs})_n/(\mathrm{AlAs})_n$ superlattices. A detailed comparison of the bulk properties calculated with these empirical pseudopoten-

Ref. 48. An important aspect of this pseudopotential is that the arsenic potential depends on the identity of its four nearest neighbors, i.e., the number of Al and Ga atoms around it.

$V(\mathbf{r})$ changes from GaAs-like to a mixed GaAlAs type at the interface and finally to AlAs-like. Thus, while $V(\mathbf{r})$ is not calculated self-consistently, it was constrained to correctly describe LDA-calculated superlattices via introduction of such interfacial effects. This feature distinguishes our empirical pseudopotential calculations from other calculations of superlattices (see review of other calculations in Ref. 48).

Equation (4) is solved by expanding $\psi(\mathbf{r},\mathbf{k})$ in plane

$$\psi_j(\mathbf{r},\mathbf{k}) = \sum_G^{G_{\max}} A_j(\mathbf{k},\mathbf{G}) e^{i(\mathbf{k}+\mathbf{G})\cdot\mathbf{r}}, \qquad (6)$$

matrix elements of $V(\mathbf{r})$ in the basis set of Eq. (6) are calculated by a Fourier transform, with no approximation except truncation: The basis set (6) is truncated at some maximum value of $G_{\max}=2.24$ a.u. (resulting in about 30 plane waves per atom in GaAs/AlAs systems) determined in the construc-

3D problem. Note also that no use is made of effective-mass, $k \cdot p$, or envelope-function approximations here.

2. Solving the Schrödinger equation

Substitution of the plane-wave expansion of Eq. (6) into the Schrödinger equation Eq. (4) results in a matrix (secular) equation whose dimension is $N_G \times N_G$, where N_G is the number of plane waves entering Eq. (6). In practice, this

$N \sim 1000$ ML. Standard techniques for solving Schrödinger's equation require orthogonalization of each state to all other states, thus leading to an N_G^3 scaling of the effort involved.

$$[-\tfrac{1}{2}\nabla^2 + V(\mathbf{r}) - \epsilon_{\mathrm{ref}}]^2 \psi_j(\mathbf{r},\mathbf{k}) = (\epsilon_j - \epsilon_{\mathrm{ref}})^2 \psi_j(\mathbf{r},\mathbf{k}), \qquad (7)$$

where ϵ_{ref} is an arbitrary "pointer" and $\{\epsilon_j, \psi_j\}$ are identical

(7) corresponds, however, to the eigenvalue closest to ϵ_{ref}. Thus, by placing the "pointer" ϵ_{ref} inside the band-gap region, one is guaranteed to find the valence-band maximum

problems can be solved readily. Reference 49 provides tech-

rithm used to solve Eq. (7). The solutions of Eq. (7) obtained this way are *exact*, equalling those of Eq. (4).

B. One-dimensional envelope-function model

In this subsection, we describe the effective-mass model used in addition to the pseudopotential method to calculate the electronic structure of the disordered SL. By using the effective mass model, we are able to find the eigenstates even far away from the band edge and obtain statistical properties of the states by calculating many different random se-

Using the Kronig–Penney effective mass model, the three-dimensional problem of Eq. (4) is reduced to the one-dimensional problem

$$\left[-\frac{1}{2}\frac{d}{dz}\frac{1}{m^*(z)}\frac{d}{dz} + V_{\mathrm{ext}}(z) \right] \phi_i(z) = \epsilon_i \phi_i(z). \qquad (8)$$

Here $m^*(z)$ is the effective mass, $V_{\mathrm{ext}}(z)$ is the external potential [to be distinguished from the microscopic atomic potential of Eqs. (4) and (5)] and $\phi_i(z)$ is the envelope func-

effective mass $m^*(z)$. Like in the empirical pseudopotential calculation, we assume periodic boundary conditions for the supercell. This is equivalent to connecting the left-hand end of the SL with its right-hand end. Written in the form of Eq. (8), we imply that the boundary condition at the GaAs/AlAs interface is the continuity of $\phi_i(z)$ and $m^*(z)^{-1}(d/dz)\phi_i(z)$. More explicitly, we have

$$\left(m^{*-1}\frac{d\phi(z)}{dz} \right)_{\mathrm{GaAs}} = \left(m^{*-1}\frac{d\phi(z)}{dz} \right)_{\mathrm{AlAs}}, \qquad (9)$$

layer both m^* and V_{ext} are constants. Let us denote by l the layer index ($l = 1, \dots N$, running from left- to right-hand side). Then, m_l^*, V_l, and the layer length d_l specify the physical

$$\left(\begin{array}{c} \phi(z_l) \\ \vdots \end{array} \right)$$

(where z_l is the left-hand-side position of the lth layer), then from Eq. (8) A_{l+1} is given by

For $E \geq V_l$ and $k = \sqrt{2m_l^*(E-V_l)}$, we have

$$M_l(E) = \left(\begin{array}{cc} \cos(kd_l) & \sin(kd_l)/k \\ -km_{l+1}^* \sin(kd_l)/m_l^* & m_{l+1}^* \cos(kd_l)/m_l^* \end{array} \right),$$

(12)

while for $E < V_l$ and $k = \sqrt{2m_l^*(V_l-E)}$ we have

$$M_l(E) = \left(\begin{array}{cc} \cosh(kd_l) & \sinh(kd_l)/k \\ & \end{array} \right),$$

$$A_{N+1} = \left(\prod_{l=1}^{N} M_l(E) \right) A_1 = A_{1'}.$$

(14)

The ith solution of E yields ϵ_i whereas the ith solution of A_l yields $\phi_i(z)$.

and scan $d(E)$ within the interesting range of E. A change of sign in $d(E)$ when E increases indicates a solution. Then Newton's iteration method is used to find the exact E value which yields the zero of $d(E)$. However, for the d-SL, when E is close to the band edge, this procedure is numerically unstable for large N due to the typical exponential growth of $\Pi_{l=1}^{N} M_l(E)$ as a function of N. In this case, we need another procedure to find localized states. We start with $A_1 = [0,1]$ and scan $A_{N+1}(E) = [a(E), b(E)]$ as a function of E. Then

if $\phi(z_l)$ belonging to this E has large amplitude near $l=1$ or

culated by shifting the starting (the ending) position from $l=1$ ($l=N$) to another point, so that this localized state is in the middle of the starting and ending points.

By switching between the above two procedures, we can reliably calculate all the states of a one-dimensional system for almost arbitrarily large N.

To solve the 1D problem we need to determine the external potential V_{ext} (i.e., band lineups) and effective masses,

are given in Fig. 6. Since the AlAs X_{1c} state is near the CBM, for small period superlattice, the X valley derived electron state could be important. For large period superlattices, the absolute CBM is the GaAs Γ_{1c} state, thus Γ valley derived electron states are important. Thus, for electron
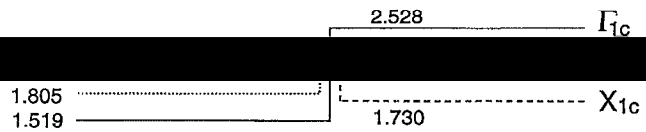

GaAs   AlAs

FIG. 6. Band offsets (eV) used for the GaAs/AlAs interface. These band edge energies yield their corresponding potential $V(z)$ in the effective-mass calculation of Eq. (8).

states, we calculate states derived from Γ and X valleys. The L valley derived states is also calculated in some cases, to

pseudopotential for the (001) and (111) directions using $m^* \approx \Delta k^2 / 2\Delta E$ are shown in Table I. Using the band offsets of Fig. 6 and the masses given in Table I, we can calculate the electronic structure of superlattices using the EMA of Eq. (8).

In this section we discuss the following cases:

(a) The ideal ordered superlattice of period n. Here $R=0$ and $p(n') = \delta(n'-n)$. This will establish the electronic structure of our "unperturbed system" (Sec. IV A);

TABLE I. EPM effective masses (in units of free electron mass) at different valleys along different directions. The GaAs X valley energy minimum is at $(0.89,0,0)(2\pi/a)$, where a is the lattice constant. Its effective mass is evaluated at this energy minimum point. All other valley minima are at their corresponding high-symmetry k points.

	Γ	X	L
GaAs (100)	0.416	0.079	0.077
GaAs (111)	0.975	0.065	0.077
AlAs (100)	0.439	0.157	0.158
AlAs (111)	1.020	0.111	0.158

X valley: (100)			
	Parallel: [100]	Perpendicular: [010]	Along [111]
GaAs	1.912	0.246	0.3466
AlAs	2.104	0.262	0.371

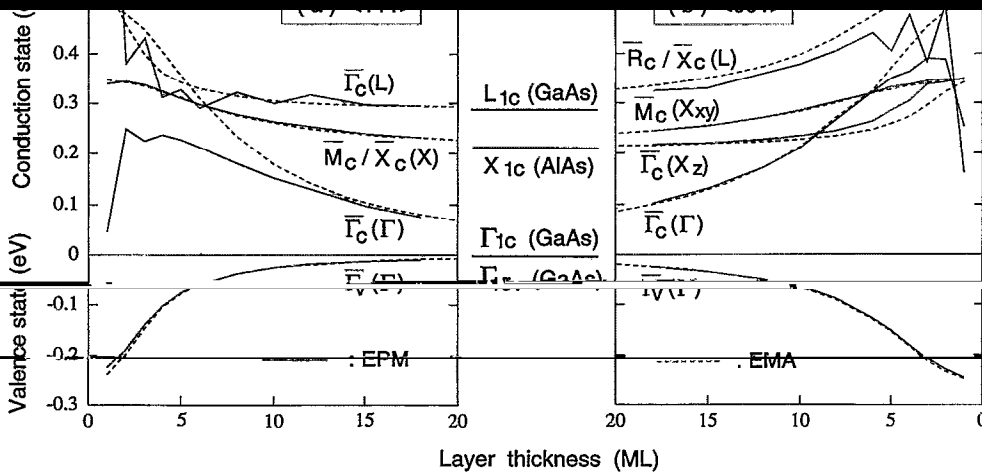| L valley: $\frac{1}{2}(111)$			
	Parallel: [111]	Perpendicular: [$\bar{2}$11]	Along [100]
GaAs	1.664	0.128	0.183
AlAs	2.120	0.168	0.242

FIG. 7. Energy levels of ideal $(AlAs)_n/(GaAs)_n$ superlattices along (a) $\langle 111 \rangle$ and (b) $\langle 001 \rangle$, as a function of period n. Solid lines: pseudopotential results; dashed lines: effective-mass results. The bulk levels in the middle column are reached asymptotically as $n \to \infty$. The SL states are denoted with an over bar,

(b) SLs with laterally intermixed interfaces. Here, the

(Sec. IV B);

(c) The single δ-doping layer case. Here, a monolayer of
This will establish the existence of bound states due to

SL (Sec. IV C);

This case will establish the electronic structure of the

stitutional randomness, and includes the disordered SLs considered by Sasaki et al.,[15] and the partially ordered ones by Arent et al.[45] (Sec. IV E).

A. Ideal periodic AlAs/GaAs superlattices: Abrupt interfaces

ergy levels on the period n, for (001)- and (111)-oriented SLs. The results correspond to the scalar-relativistic limit without spin-orbit interaction. Since we do not use envelope functions, the results are not limited to near zone center
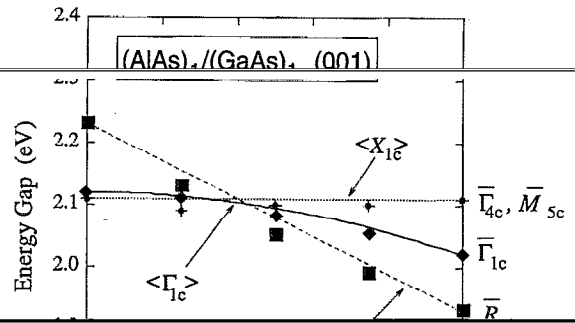
all period n. Both the highest valence and the lowest con-

(ii) The second conduction band at Γ, i.e., $\Gamma(L)$, is folded from the zinc-blende $\Gamma - L_z$ line. For small n, this pseudodirect $\bar{\Gamma}_c(L_z)$ state mixes strongly with the direct $\bar{\Gamma}_c(\Gamma_c)$ state. The mixing, and thus the level repulsion, shows

tion of repelling states on the same or on either sublattice[52]).

middle column of Fig. 7).

The situation is very different for (001) oriented ideal

point $\bar{K}$,

(ii) For $n < 4$, the lateral $X_{x,y}$ valleys (folded to $\bar{M}$) and the X_z valley (folded to $\bar{\Gamma}$) are nearly degenerate;[54]

(iii) For $1 < n \leq 8$ the pseudodirect, AlAs-like $\bar{\Gamma}_c(X_z)$ state is below the direct, GaAs-like $\bar{\Gamma}_c(\Gamma_c)$ state, thus the SL is type II;[55] for $n > 8$, however, $\bar{\Gamma}_c(\Gamma_c)$ is lower, so the system is type I (experimentally, the type-II/type-I crossover is found[54] at $n \approx 11$).

compared in Fig. 7 (dashed lines) with the EPM results (solid lines). The effective masses used in the EMA are from Table I which is calculated from the EPM. At large superlattice period n, the EMA results agree very well with the EPM results. [For the (001) $\bar{R}/\bar{X}(L)$ curve, there is a small dis-

agreement with previous theoretical LDA studies. We find

(iii) the potential offsets for the GaAs/AlAs interface are small (Fig. 6), thus, even for $n=1$, the k in Eqs. (12) and (13) is small, so nonparabolicity is small.

In contrast to the good agreement between EMA and EPM for the above states, the EPM $\bar{\Gamma}_c(\Gamma)$ curve for both (001) and (111) bends down at small n, while in the EMA there is a monotonic dependence. The EPM bending is due to the mixing of $\bar{\Gamma}_c(\Gamma)$ with $\bar{\Gamma}_c(X_z)$ in the (001) case and with $\bar{\Gamma}_c(L)$ in the (111) case.[52] This cannot be described by the one-band effective mass model (or even four-band $k \cdot p$
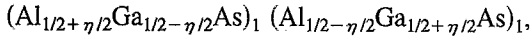

and the broken lines are linear interpolations between the respective end

1. Intermixing in (001) superlattices

Chemical nonabruptness of interfaces in short-period superlattices has been suggested by Laks and Zunger as a reason for the discrepancy between the experimental assignment of the conduction-band minimum and theoretical predictions. In particular, for the monolayer $(n=1)$ superlattice

given supercell. $\langle \bar{\Gamma}_{1c} \rangle$, $\langle X_{1c} \rangle$, and $\langle L_{1c} \rangle$ are shown in Fig. 8 for $n=0$, 0.25, 0.50, 0.75, and for the perfect monolayer

X -derived gap at $\bar{M}$ is found.[54] We tested the idea of Laks

$n \approx 0.4$, in close agreement with the LDA result[57]

$$(\mathrm{Al}_{1/2+\eta/2}\mathrm{Ga}_{1/2-\eta/2}\mathrm{As})_1 \, (\mathrm{Al}_{1/2-\eta/2}\mathrm{Ga}_{1/2+\eta/2}\mathrm{As})_1,$$

where η is the long-range-order (LRO) parameter. $\eta=1$ de-

2. Intermixing in (111) superlattices

As the repeat period n of the ideal SL increases, chemi-

roughness in the monolayer superlattice we expand the repeat period $(X \times Y)$ in the interface plane to an (8×8) unit cell. We can thus have $\eta = 1 - n/32$, where n is the number

the band gaps can shift considerably. We have considered the $(\mathrm{AlAs})_6/(\mathrm{GaAs})_6$ (111) SL, because of a controversy about the nature of the band gap between theory[52,60]

however, we assume a repeat period of 4 ML along [001], resulting in a 512 atom supercell. Hence, within the supercell there are four distinct Al-rich and four distinct Ga-rich lay-

SL, we have used a planar (4×4) unit cell to simulate chemical intermixing within ± 1 ML across the interfaces, resulting in a 384 atom 3D unit cell. The superlattice is thus converted

AlAs layers, and two alloy layers. We chose the composition lyzed in terms of their "parent" zinc-blende states from of the alloy layers to be 50%, corresponding to maximum

expanded in terms of a usually small number of zinc-blende latter expansion as weights in evaluating spectral averages of zinc-blende-like eigenvalues.[59] For example, $\langle \bar{\Gamma}_{1c} \rangle$ denotes

the pseudodirect $\bar{\Gamma}_{6c}(L_{6c})$ and indirect gaps $\bar{M}_{6c}(X_{6c})$

however, does not change upon intermixing, remaining $\bar{\Gamma}_{6c}(\Gamma_{6c})$ although the pseudodirect transition $\Gamma_{6c}(L_{6c})$ is now only 20 meV (down from 50 meV) away.

Gap (ZB origin)	Ideal SL	Intermixed
$\bar{\Gamma}_{6c}(\Gamma_{6c})$	1.81	1.89
$\bar{\Gamma}_{6c}(L_{6c})$	1.86	1.91
$\bar{M}_{6c}(X_{6c})$	1.92	1.95
$\bar{M}_{6c}(L_{6c})$	2.02	2.04

Experimentally, the absorption edge was determined to be at 1.90 eV,[61] close to our calculated band gap of the intermixed SL. The observed PL emission peak at 1.80 eV, however, cannot be explained by chemical intermixing: Table II shows that intermixing leads to a blue shift while experimentally the PL is red shifted. A possible explanation for a large red shift of the PL emission is offered in Sec. IV E, where it is

FIG. 9. Pseudopotential calculated planar average of the wave functions

C. A single δ layer inside an ordered superlattice

We next model the case of a single layer of A or G inserted in an ordered A_2/G_2 SL. It is well known[62] that, while in 3D an impurity potential has to exceed a certain

bound state. To understand the possibility of impuritylike localization, consider, for example, a G_3 δ layer embedded in the otherwise perfect o-SL $\cdots A_2G_2A_2G_2A_2G_2\cdots$, thus converting it into $\cdots A_2G_2A_2G_3A_2G_2\cdots$, denoted as $A_2/G_2{:}G_3$. If the G_3 δ layer is attractive to electrons (holes) it will bind a state below the CBM (above the VBM) of the o-SL.[63] We find that a (GaAs)₃ δ layer in the (AlAs)₂/(GaAs)₂ o-SL indeed binds an electron and a (double degenerate) hole [Fig. 9(a)], while an (AlAs)₃ layer binds an electron but does not bind a hole (Fig. 10). Figure 11 shows as dashed lines the dispersion of the bound states of a single δ layer in A_2/G_2.

lowing length scales (in ML units). The effective localization length for wave function ψ_E at energy E is defined as[64]

$$L_{\text{eff}}(E) = \frac{1}{d}\left[\int dz\left(\int dx\,dy|\psi_E(\mathbf{r})|^2\right)^2\right]^{-1}, \quad (16)$$

of the $n=2$ ordered SL along the symmetry lines $\bar{\Sigma}$ and $\bar{\Delta}$, i.e., from $\bar{\Gamma}$ to $\bar{M}=1/\sqrt{2}(1,1)$ and from $\bar{\Gamma}$ to $\bar{X}=1/\sqrt{2}(1,0)$, respectively. The thin horizontal lines denote the band edges

therefore correspond to a bound state. For the δ layer, we

while those of $A_2/G_2{:}A_3$ are $\Delta\varepsilon_e=33$ and 5 meV, respectively. The hole binding energy of $A_2/G_2{:}G_3$ is $\Delta\varepsilon_h=37$

(GaAs)₂/(AlAs)₂ are extended states, as illustrated in Fig. 9(b) for the next higher (lower) state following the bound electron (hole) in $A_2/G_2{:}G_3$.

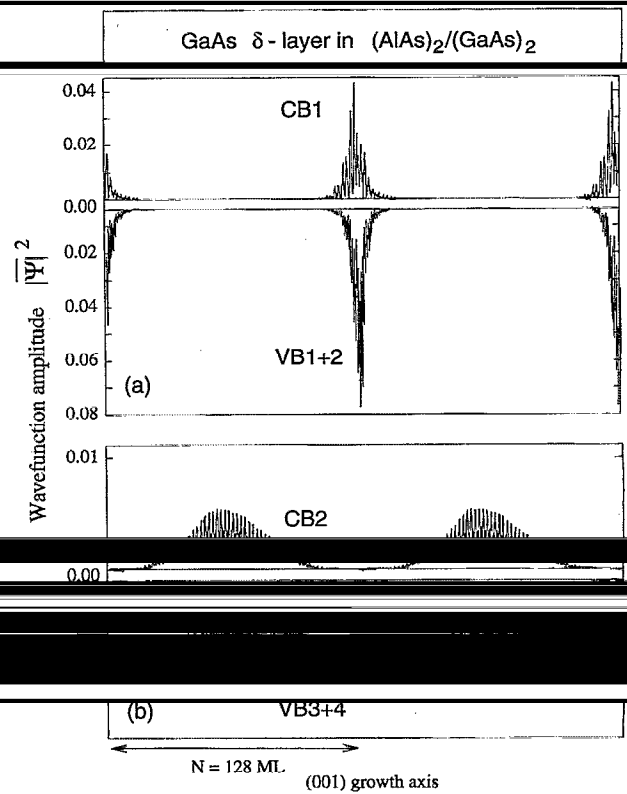The wave-function localization perpendicular to the

FIG. 10. Like Fig. 9, but for an (AlAs)₃ δ layer. In this case, there is no

CBM of periodic δ-layers

CBM

δ-layer

o-SL

po-SL

d-SL

VBM

po-SL

VBM of periodic δ-layers

VBM of o-SL

Degree of Disorder R

FIG. 12. Pseudopotential calculated band-edge energies of disordered [d-

supercell size is $N=128$.

function of R [Eq. (3)]. Lines are guides to the eye. The thick horizontal lines denote the unperturbed band edges of the parent o-SL. The vertical bars on the d-SL data points denote the range of binding energies obtained from ~ 10 different realizations of a d-SL with length $N=128$.

and measures the region along z where ψ_E is "sizeable." In Eq. (16) the planar average of $|\psi_E|^2$ is taken before integrating along z, d is the monolayer thickness, and the wave function is assumed to be normalized in the volume of the

similar to those obtained in the fully disordered SL, suggesting that the same mechanism of localization could be at work

whereas a state that is completely confined to one monolayer has $L_{eff}=1$. The asymptotic decay length γ^{-1} far away from the localization region is given by $\langle|\psi_E(z)|\rangle \propto e^{-\gamma z}$, where

D. An ordered array of δ layers inside an ordered superlattice

TABLE III. Effective localization length L_{eff} [Eq. (16)] and exponential decay length γ^{-1} for the δ-layer systems depicted in Figs. 9 and 10, and the disordered and partially ordered SLs depicted in Figs. 15 and 16, respectively. Reported are the values for the states at the conduction-band minimum (CBM) and at the valence-band maximum (VBM) in ML units.

as the thin solid line in Fig. 12. We see that even for an array of closely spaced δ layers ($R \to 1$) the binding energy does not increase, indicating negligible interaction between the neighboring, coherently arranged bound states. In fact, at

those of a disordered system. Consequently, short supercells

	L_{eff}	γ	L_{eff}	γ

TABLE IV. Overview of different disordered systems [superlattices (SL) and multiple quantum wells (MQW)] in the parameter space of R [Eq. (3)] and $\Delta n/n$.

	Small mean density	Large mean density
Small fluctuation ($\Delta n \ll n$)	nearly "ideal" SL/MQW impuritylike localized states	strongly disordered MQW effective-mass-like bound states
Large fluctuation	Strong perturbation of band edges	d-SL, po-SL
$n < 10$		

with $N \approx 10$–20, as have been used before to describe disor-
dered SLs [39] are unable to simulate the behavior of truly

E. A disordered array of δ layers

Next, we introduce disorder in the SL by arranging the δ

that very large supercells are required, if one wishes to ac-
curately describe the layer–layer correlation function of a
disordered system. We have used total lengths N of up to
1000 ML for EPM, and up to 2000 ML for EMA calcula-
tions, in order to verify the convergence of the results ob-

est needs to be evaluated; in some cases (see below) we have
used ~10 realizations of a d-SL of given total length N and
disorder parameter R, and have found that the EPM-

lengths) have very small fluctuations. Therefore, we have
often used a single realization of a d-SL to calculate band-
edge energies and wave functions. For the EMA-calculated
density of states, on the other hand, we have performed con-

In the following, we discuss separately two regimes of

thickness fluctuations Δn are of the same order as the unper-
turbed thickness, i.e., $\Delta n \approx n$. This case includes the d-SLs
of Sasaki et al. and the po-SLs of Arent et al. Second, we
treat the case where the thickness fluctuations are relatively
small perturbations of the ideal SL, i.e., $\Delta n \ll n$. An overview
of the different regimes considered is given in Table IV.

1. Disordered SLs with $\Delta n \approx n$: EMA density of states

To calculate the spectral properties of a d-SL over a
large energy range, we use the effective-mass model de-
scribed in Sec. III B. The advantage of the EMA method is
that we can easily calculate a large number of eigenstates
(not only near-gap states). This permits obtaining a good

properties. We have thus modeled a 2000 ML Sasaki-type

edges. We calculated heavy-hole states for the hole and X

13. Each state is represented by a single horizontal line. The
vertical position of the line indicate its energy and horizontal

line is $2L_{\text{eff}}$ using the one-dimensional version of Eq. (16).
Figure 13 shows that all states are localized, as expected

There is no transition from localized states to delocalized
states. Around the band edge, the localization of the states is
more properly described by the Lifshitz theory. Figure 13
gives the distribution of the d-SL states, in both energy and

One way to display the information in Fig. 13 more
quantitatively is to calculate the density of states (DOS) and
localization length L_{eff} as functions of energy E. We have
calculated 100 d-SL systems (each with 2000 ML as in Fig.

here are the DOS considering the Γ point only, thus, a
one-dimensional DOS. If the lateral dimensions were consid-
ered, the shapes of the DOS would change.) For electron
states, we calculated both the X valley states and Γ valley

only makes sense for low-energy regions where two separate
valleys are well defined. For high-energy regions, the states
from X and Γ valleys may not be distinguishable, and thus
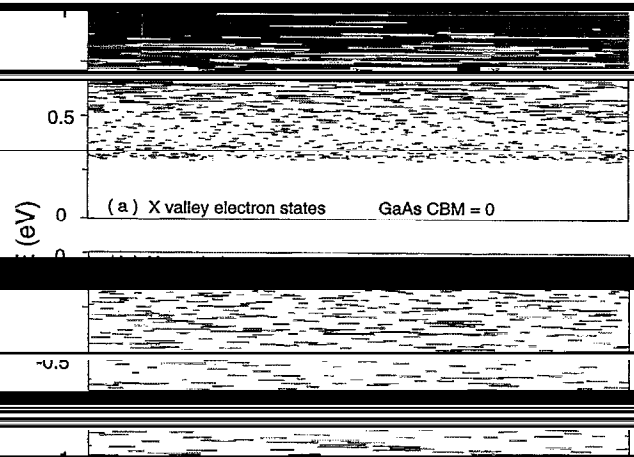are not well defined. They may correspond to a single state in

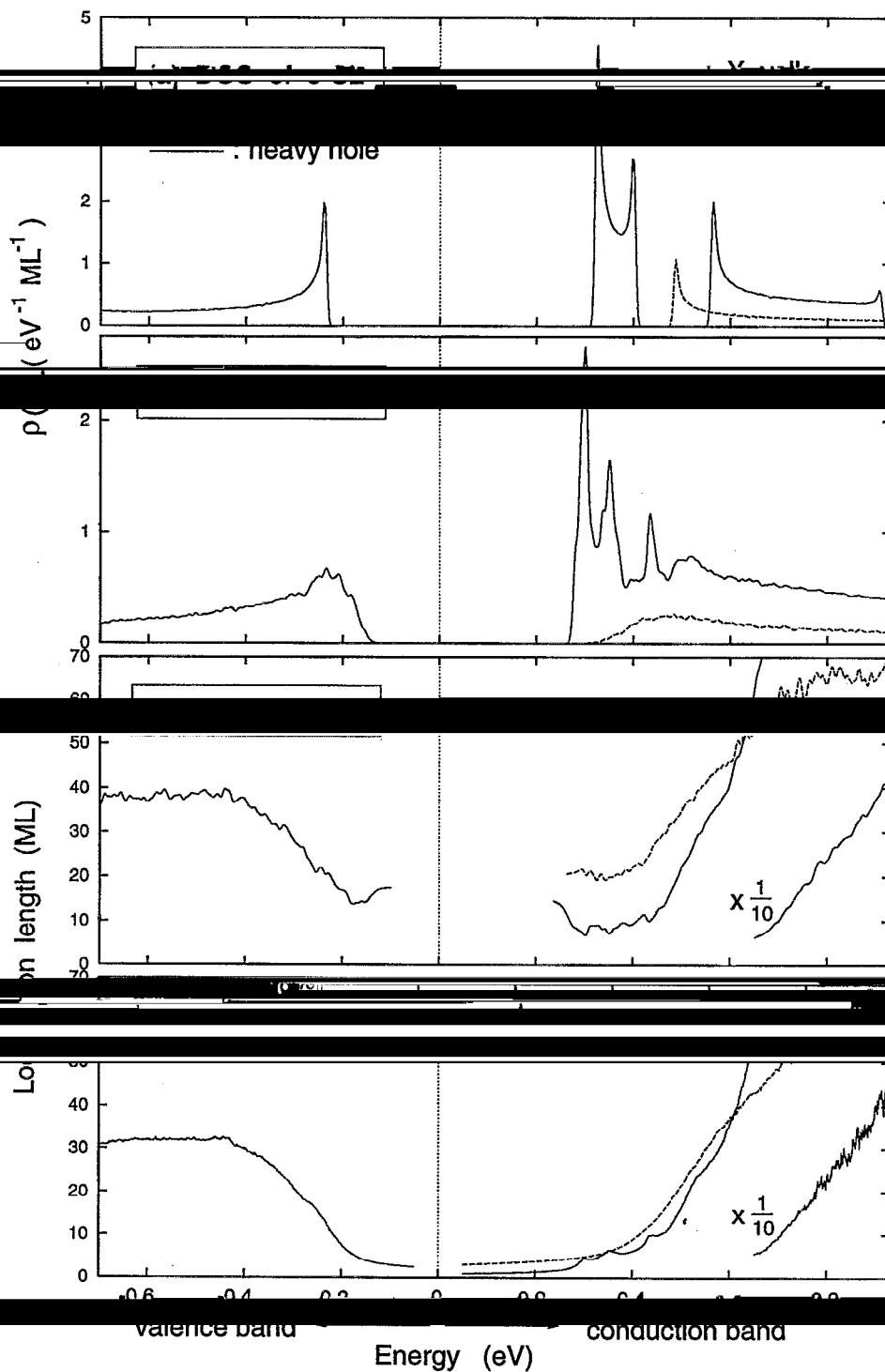FIG. 13. Effective-mass calculated localized states of a 2000 ML d-SL.

FIG. 14. Effective-mass calculated density of states of (a) the (001)-ordered $(GaAs)_2/(AlAs)_2$ and (b) Sasaki-type disordered superlattices, and the localization lengths (c) L_{eff}, (d) γ^{-1} of the disordered superlattice. The conduction-band energy is measured from the bulk GaAs CBM and the valence-band energy is measured from the bulk GaAs VBM.

a multiband calculation. A very interesting fact is the peaks in the DOS of X valley electronic states. To understand these peaks, we have calculated the DOS for the $(GaAs)_2/(AlAs)_2$ ordered superlattice. The results are shown in Fig. 14(a). It is evident that the peaks of X valley states of the d-SL in Fig. 14(b) are the remnants of the peaks seen in Fig. 14(a) for the o-SL with some shifts. On the other hand, for Γ valley states

and heavy-hole states, there is only one peak in the ordered superlattice, thus their DOS of d-SL have simple structures.

The effective localization length L_{eff} [Eq. (16)] is shown in Fig. 14(c). Notice that L_{eff} increases a bit near the band edge. As described by the Lifshits theory, this phenomenon is due to consecutive wide potential wells. At energy far away from the band edge, L_{eff} of the X valley electron states and

heavy-hole states bend down. Part of the reason is that we used the boundary condition of Eq. (9). As a result, for very large E, when the effect of the potential is no longer important, the mass confinement still plays an important role. This

length γ^* as described in Sec. IV C. It turns out that this γ is just the exponential growth rate of $A_{N+1}(E)$ [defined in Eq. (14), which does not equal A_1 for arbitrary E] as a function of N. If E is an exact eigenvalue ϵ_i of an localized state, then $A_{N+1} = A_1$, thus, the magnitude of A_{N+1} is O(1). How-

$A_{N+1}(E)$ directly and the result is accurate and reliable. The $\gamma^{-1}(E)$ are shown in Fig. 14(d). Note that, in the DOS tail region, L_{eff} is larger than $2\gamma^{-1}$, indicating Lifshits localiza-

This can be understood by the fact that $L_{\text{eff}} \approx 3\gamma^{-1}$ for a localized wave function $\cos(kz)e^{-\gamma|z|}$ with k much larger than

the dips of $L_{\text{eff}}(E)$ and peaks of $\gamma^{-1}(E)$ can be understood as follows. The existence of the eigenstates around a given

induce a peak in $\gamma^{-1}(E)$. On the other hand, because of

2. Disordered SLs with $\Delta n \approx n$: Band-edge states and oscillator strength

We now focus on the band edges near the band-gap re-

and emission in the visible-light and near-infrared regions,

d-SLs. First, we discuss the results of our pseudopotential calculations. In Fig. 11 we show the EPM-calculated dispersion of the band-edge states of the d-SL (solid lines) with $p(1) = p(2) = p(3) = \frac{1}{3}$ along the symmetry lines $\overline{\Sigma}$ and $\overline{\Delta}$. The thin horizontal lines denote the band edges of the under-

("binding energy") increases in the order $M \to \Gamma \to X$. The large binding energy at $\overline{X}$ is a consequence of the level re-

pulsion of the folded L_{1c} states, which is much stronger for odd values of the repeat period n than for even n [see Fig. 7(b)]. In the d-SL the odd–even selection rule is broken, leading to a stronger level repulsion in the d-SL than in the

the conduction-band edge below the ones at $\overline{X}$ and $\overline{M}$ by 60 meV, making the d-SL a direct-gap material, even though the o-SL is indirect (with CBM at $\overline{M}$).

show a few band-edge wave functions of an $N=1000$ ML d-SL, which are plotted using the planar average introduced in Fig. 9. For example, the states labeled CB3 and VB1 are localized at the same positions along the chain, and conse-

tor strength f of an optical transition, which is defined as

$$f = \frac{1}{\hbar\omega} \frac{2|\langle c|\mathbf{p}|v\rangle|^2}{3m}. \tag{17}$$

Here $\hbar\omega$ is the transition energy, $\langle c|\mathbf{p}|v\rangle$ the dipole matrix

average over the three polarizations x,y,z. In Table V we report calculated values of f for direct transitions in various

(i)   oscillator strength of pseudodirect transitions in ordered SLs are 1–2 orders of magnitude smaller than those of the (higher energy) direct transitions.

(ii)   The transition between an extended state and a local-

is of the similar strength as a pseudodirect transition,

(iii)   Transitions between two states that are localized in the same region along z are of comparable strength

Thus, the transition between the two localized states VB1

late $\tau = 1$ ns for the VB1$\to$CB3 transition at energy 1.96 eV. These radiative lifetimes are 1000$\times$ faster compared to those measured in indirect-gap o-SLs ($\tau \approx 5.5$ μs at $T=2$ K).[54]

well with measured PL emission lines in d-SLs, which were

We have seen that in ordered SLs the distinction between direct and pseudodirect transitions can be made by mapping SL states on "parent" states in the zinc-blende structure: Pseudodirect transitions at a SL wave vector $\overline{\mathbf{K}}$ involve one folded state and one state genuine to $\overline{\mathbf{K}}$. An example is the

(the height of the d-SL Brillouin zone is equal to $2\pi/Nd$), the parentage of a d-SL state can still be defined in terms of its projection on zinc-blende states. We have performed such an analysis for a few conduction-band-edge states in (001) d-SLs. We found two types of states:

(i)   localized states whose projection on zincblende (ZB) states is peaked at the Γ point, and

(ii)   localized states whose projection is peaked at the X_z point of the ZB Brillouin zone.

In real space, the Γ-like states are localized in GaAs-rich regions [e.g., where a few (GaAs)$_n$ layers are separated by

(a) EMA Γ electron

CB3=0.3858 CB1=0.3824 CB2=0.3828

(b) EMA X electron

CB2=0.2684 CB1=0.2595

(d) EPM hole

VB2=-0.1676 VB1=-0.1673
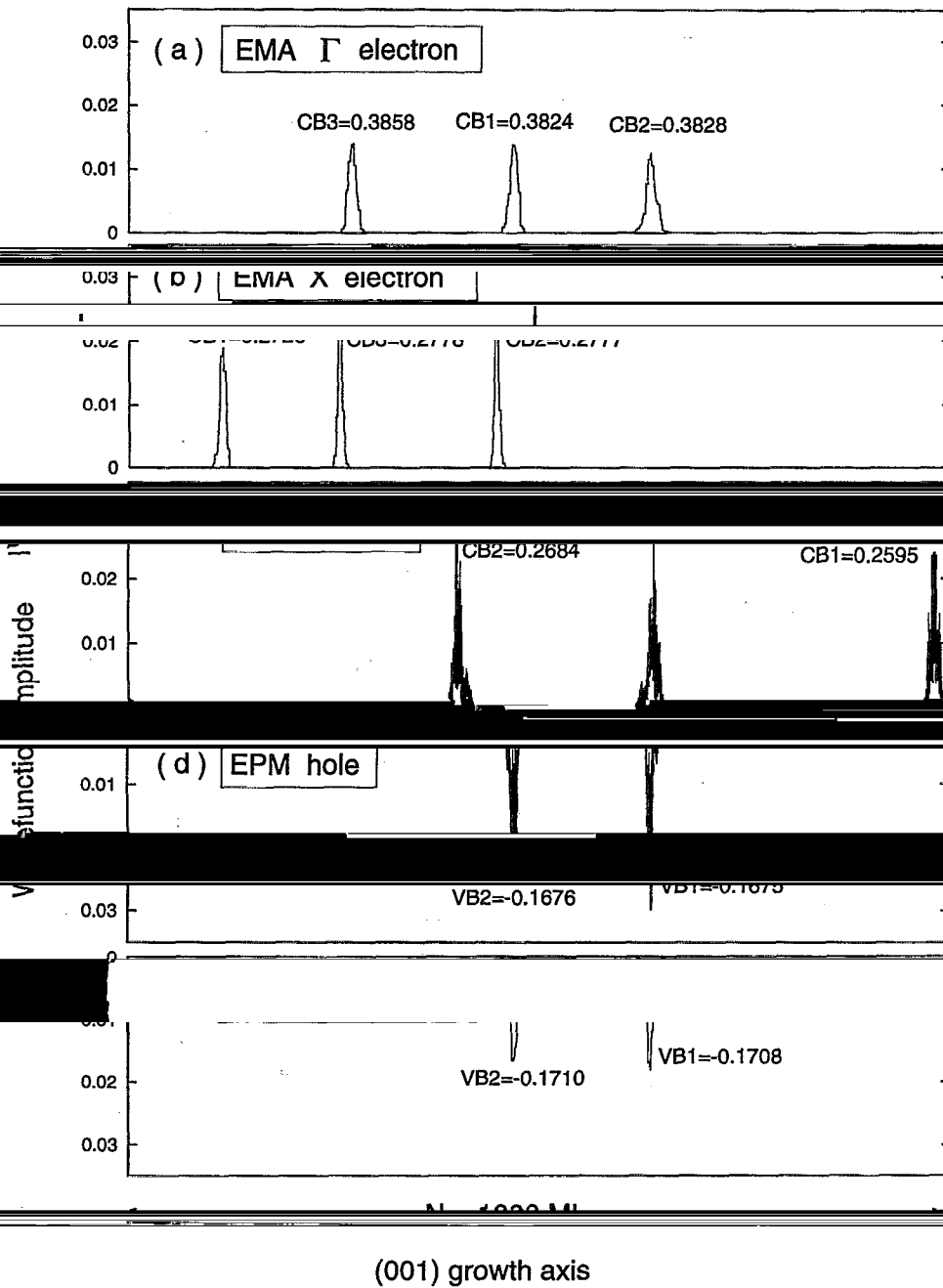
VB2=-0.1710 VB1=-0.1708

(001) growth axis

FIG. 15. The valence-band maximum states and conduction-band minimum states of a 1000-ML disordered superlattice, obtained by empirical pseudopotential model (EPM) and effective-mass approximation (EMA). The numbers are the eigenenergies of the states in eV. For the conduction-band states and valence-band states, they are measured from bulk GaAs CBM and VBM, respectively.

type-II band alignment of the ordered (001) SLs. Unlike in mechanism of localization in both cases is essentially the

are Γ-like]. Note that the 1×1 o-SL also has the $\Gamma(\Gamma_{1c})$ state below the $\bar{\Gamma}(X_z)$ state [Fig. 7(b)]. This band order is not reproduced by the EMA, and we see below that also for the

concentration of δ layers, an increasing number of bound states is introduced, which are degenerate at small concentration R. Unlike in the case of the periodic array of δ layers,

TABLE V. Oscillator strengths of direct optical transitions in bulk materials

System	Final state	Energy (eV)	f
Bulk GaAs	Γ_{1c}	1.52	4.03
$(AlAs)_1(GaAs)_1$	$\Gamma(L_1)$	2.12	2.71
$(AlAs)_2(GaAs)_2$	$\Gamma(X_z)$	2.09	0.08
GaAs δ layer	CB1	2.04	1.67
d-SL	CB3	1.96	1.68
po-SL	CB1	1.87	2.76

trons. This asymmetry is contrary to expectations based on 1D one-band models, and reflects the strong band coupling

because the kinetic energy becomes increasingly dominant

partially ordered SL (po-SL), which was studied experimentally by Arent et al.[45] The corresponding wave functions are depicted in Fig. 16. While the trends are similar to those observed in the d-SLs two distinct features are noteworthy:
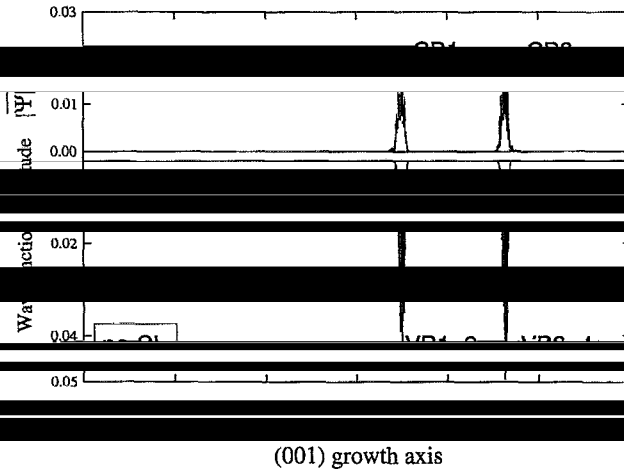
(i) Occupied and unoccupied levels with corresponding

(001) growth axis

FIG. 16. Pseudopotential calculated planar average of the wave functions

---

(ii) the band-gap reduction is slightly larger for the po-SL than for the d-SL at equal R (see Fig. 12).

Indeed, PL emission lines have been measured at energies as low as 1.87 eV,[66] in agreement with our calculated band gap of 1.87 eV. The CB1 and VB1+2 states are localized in a region where five $(GaAs)_3$ wells are separated by four

distribution function of the po-SL leads to LRO (see Fig. 4), which causes an enhancement of the structure factor $|S(k_n)|^2$

Next, we calculate the Sasaki-type d-SL using the effective-mass model. The EMA results are also shown in

wave-function shape; the eigenenergies differ by only 3 meV. The wave functions are localized at positions where consecutive wide GaAs wells are separated by thin AlAs barriers.

For electron states, the situation is more complicated. For EMA states, again, the location of the localized states is simply determined by the geometry of the potential. For example, the EMA Γ valley states in Fig. 15(a) are localized where a few consecutive wide ($n=3$) GaAs wells are separated by thin ($n=1$) AlAs barriers. Thus, these EMA Γ valley

states [Fig. 15(b)], on the other hand, are localized where a few consecutive wide ($n=3$) AlAs wells are separated by

EMA results: The d-SL has a pseudodirect band gap in the

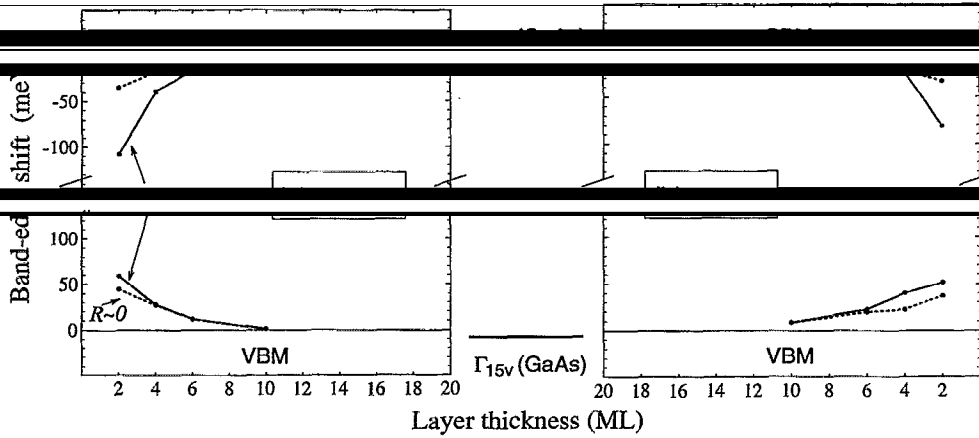derived CB2 state in Fig. 15(a). Thus, the EMA can still be useful to describe some properties of the electron state in the

FIG. 17. Pseudopotential calculated gap levels in the presence of 1 ML thickness fluctuations in $(AlAs)_n/(GaAs)_n$ superlattices along (a) $\langle 111 \rangle$ and (b) $\langle 001 \rangle$, as a function of period n. Energies are measured with respect to the band extrema of the ideal $n \times n$ SL (see Fig. 7). $R=1$ and $R \rightarrow 0$ denote, respectively, the concentrated and dilute limit of chain mutations [Eq. (3)].

Fig. 17 relative to the band edges of the ideal SLs (the energy zero, see Fig. 7). We see that:

(i) The band-gap reductions $\Delta E = \Delta \varepsilon + \Delta \varepsilon$ decay direction; they are 166, 67, 29, and 14 meV for $n=2$, 4, 6, and 10 in the $\langle 111 \rangle$ direction, and 133, 64, 36, and 27 meV in the $\langle 001 \rangle$ direction, respectively;

("band-gap pinning") of the number of chain mutations.

In order to explain these findings, we discuss the intermediate case of the $n=6$ $\langle 111 \rangle$ SL, where the VBM is already pinned (independent of R), but where the CBM still shows dispersion with R (see Fig. 17). Figure 18(a) shows the CBM and VBM wave functions for the $R=1$ SL. The minimal amplitude in the AlAs barriers and maximal amplitude on the two neighboring mutated (7 ML) GaAs wells

resembles a bound state in a coupled double quantum well. The hole wave function at the VBM is likewise localized on a number of mutated, 7 ML, GaAs wells [Fig. 18(a)]; in con-

tern of the VBM wave function is that these states are in fact decoupled, quantum-well confined states, which are degenerate in energy within the accuracy of our calculation ($\lesssim 0.1$ meV). A typical hole and electron wave function localized on an isolated $(GaAs)_7$ mutation in an otherwise ideal 6×6 $\langle 111 \rangle$ SL are shown in Fig. 18(b). We see that the hole wave

concentrated $(R=1)$ mutations [Fig. 18(a)], and its binding energy $\Delta \varepsilon_h (R \rightarrow 0) = 11$ meV equals the value at $R=1$. At the CBM, the larger penetration of the wave function into

FIG. 18. Pseudopotential calculated planar averages of wave functions squared of the CBM and VBM in the $(AlAs)_6/(GaAs)_6$ SL along $\langle 111 \rangle$ with ± 1 layer-thickness fluctuations. Hole wave functions are plotted in the

a 6×6 SL host. The rectangular lines show the growth sequence of the SL, with GaAs layers represented by wells, and AlAs layers represented by barriers, respectively. The vertical arrows in (a) indicate the 7-ML-thick, "mutated" wells.

states should be observable as photoluminescence centers whose energy is below the absorption edge of the underlying "ideal" SL structure. This photoluminescence will lack pho non lines because the optical transitions are direct in the

good quantum number), and because the k_z selection rule is relaxed by vertical disorder. Indeed, while we have shown in Sec. IV A that ideal $\langle 111 \rangle$ $(AlAs)_n/(GaAs)_n$ SLs have a direct band gap with a type-I band arrangement, Cingolani and co-workers[61] noted a ~100 meV red shift of the photoluminescence at 1.80 eV relative to the absorption in

the red-shifted photoluminescence originates from thickness-fluctuation bound states. Our calculated band gap of the $n=6$ superlattice with ± 1 ML thickness fluctuations is 1.78 eV for $R=1$, and 1.80 eV for $R \to 0$, close to their observed photoluminescence peak position (1.80 eV).[61] Recall that chemical intermixing leads to a blue shift of the band gap (see Table II), whereas larger thickness fluctuation is needed to explain the observed 100 meV red shift.

Figure 17 shows that the bound states of isolated mutations $(R \to 0)$ merge with those of concentrated layer-thickness fluctuations $(R \to 1)$ at some pinning period n_p. At this point the band-gap reduction is pinned at the value

$$\Delta E_g(R) = \lim \Delta E_g(R) = \Delta \varepsilon_e + \Delta \varepsilon_h, \qquad (18)$$

where $\Delta \varepsilon_e$ $(\Delta \varepsilon_h)$ is the electron (hole) binding energy of an isolated $(R \to 0)$ layer mutation. Qualitatively, Eq. (18) can be understood in terms of the 1D effective-mass picture (Sec. III B). Each of the $(n+1)$ ML mutations gives rise to a bound state below the band edge of the $n \times n$ SL.[20,14] For very large n, when the quantum wells are completely decoupled (the tunneling probability and, hence miniband width, decrease exponentially with n), the SL energy spectrum is simply that of degenerate single quantum wells of thicknesses n' with eigenenergies $\varepsilon_\nu(n')$. Hence, the extra binding energy of an $(n+\Delta n)$ ML mutation approaches asymptotically

where $\varepsilon_0(n)$ is the ground-state energy of a carrier with mass m^* in an n-ML-wide quantum well, which scales like

rather than a fixed Δn, we obtain from the first equality of Eq. (19) $\Delta \varepsilon_e = 10.0, 2.4,$ and 0.7 meV for $n=20, 50,$ and 100 in the $\langle 111 \rangle$ SL [the last equality of Eq. (19) gives 14.3, 3.0, and 0.8 meV, respectively]. The band-gap reduction for a

V. CONCLUSIONS

Our main conclusions can be summarized as follows.
(a) (001)-ordered superlattices:

(i) The $n=1$ SL has an indirect band gap at $\bar{R}$; Insufficient interfacial abruptness in the experimentally studied samples[54] leads instead to an X-derived CBM.

(ii) For $n \le 4$, the $\bar{M}(X_{xy}$-folded) states and the $\bar{\Gamma}(X$-folded) states are nearly degenerate;

(iii) The crossover from AlAs-like $\bar{\Gamma}_{1c}(X_z)$ (type II) to GaAs-like $\bar{\Gamma}_{1c}(\Gamma_{1c})$ (type I) happens around $n=8$.

(b) (111)=ordered superlattices:

(i) $\bar{\Gamma}_{1c}(\Gamma_{1c})$ is the CBM (type I) for all n;

(ii) There is a strong even-odd oscillation of the CBM energy due to mixing.

ordered SLs, Cingolani and co-workers[61] found for $n=6$ a type-II SL with a ~100 meV red shift between absorption and PL; we find that lateral interfacial intermixing can not explain this discrepancy, but monolayer thickness fluctuations in the measured sample do resolve the disagreement.

(c) Single δ layer doping in o-SL:

(i) A $(GaAs)_3$ δ layer in $(GaAs)_2/(AlAs)_2$ (001) SL produces an electron and a hole bound state with binding energies $\Delta \epsilon_e = 18$ meV and $\Delta \epsilon_h = 37$ meV, respectively;

(ii) An $(AlAs)_3$ δ layer in $(GaAs)_2/(AlAs)_2$ (001) SL pro-

(d) An ordered array of δ layers:

The bound states in neighboring δ layers start to have large interaction when their distance is less than 20 ML.

(e) A disordered SL with $\Delta n \approx n$ (i.e., $n=1,2,3$):

(i) There is a 130 meV red shift in the band gap compared with the o-SL;

(ii) The conduction-band minimum is at $\bar{\Gamma}$, not at $\bar{X}$ as for the $n=2$ o-SL

(iii) The conduction-band-edge states are more Γ-like than X-like, thus the oscillator strength is as large as the pair;

(iv) The band-edge state localization length of the d-SL is about the same (20 ML) as the δ layer bound state;

(v) The localization lengths increase as the energy moves there is no mobility edge;

(vi) The DOS of the d-SL has a peak near the edge of o-SL DOS and has a tail into the band-gap region; if

(f) A disordered SL with $\Delta n \ll n$:

For $\Delta n = 1$ and $n > 6$, the band-edge energies are nearly pinned at their δ doping level, independent of the magnitude of the disorder.

[1] A. Ourmazd, D. W. Taylor, J. Cunningham, and C. W. Tu, Phys. Rev. Lett. 62, 933 (1989).

[3] B. Jusserand, F. Mollot, R. Planel, E. Molinari, and S. Baroni, Surf. Sci. 267, 171 (1992).

[4] R. M. Feenstra, D. A. Collins, D. Z.-Y. Ting, M. W. Wang, and T. C.

N. Miller, J. Vac. Sci. Technol. B 5, 1191 (1987).

[7] R. F. Kopf, E. F. Schubert, T. D. Harris, and R. S. Becker, Appl. Phys.

Phys. Lett. 58, 2755 (1991).

[9] C. Parks, A. K. Ramdas, M. R. Melloch, and L. R. Ram-Mohan, Phys. Rev. B 48, 5413 (1993).

[10] J. R. Meyer, A. R. Reisinger, K. A. Harris, R. W. Yanka, and L. M. Mohnkern, Appl. Phys. Lett. 64, 545 (1994).

[11] J. D. Dow, S. Y. Ren, and K. Hess, Phys. Rev. B 25, 6218 (1982).

[12] S. Das Sarma, A. Kobayashi, and R. E. Prange, Phys. Rev. Lett. 56, 1280 (1986).

[13] R. Merlin, K. Bajema, R. Clarke, F.-Y. Juang, and P. K. Bhattacharya, Phys. Rev. Lett. 55, 1768 (1985).

[14] A. Chomette, B. Deveaud, A. Regreny, and G. Bastard, Phys. Rev. Lett. 57, 1464 (1986).

[15] A. Sasaki, M. Kasu, T. Yamamoto, and S. Noda, Jpn. J. Appl. Phys. 28,

[16] C. A. Warwick and R. F. Kopf, Appl. Phys. Lett. 60, 386 (1992).

[17] V. I. Belitsky, T. Ruf, J. Spitzer, and M. Cardona, Phys. Rev. B 49, 8263 (1994).

[18] C. A. Warwick, W. Y. Jan, A. Ourmazd, and T. D. Harris, Appl. Phys. Lett.

M. J. S. P. Brasil, R. A. Bernussi, M. A. Cotta, M. V. Marquezini, J. A.

[20] R. K. Littleton and R. E. Camley, J. Appl. Phys. 59, 2817 (1986).

[21] H. X. Jiang and J. Y. Lin, Superlattices and Microstructures 3, 689 (1987).

[22] R. A. Davies, M. J. Kelly, and T. M. Kerr, Appl. Phys. Lett. 53, 2641 (1988).

Sci. Technol. A 11, 923 (1993).

[28] M. Proctor, G. Oelgart, H. Rhan, and F.-K. Reinhart, Appl. Phys. Lett. 64, 3154 (1994).

[29] P. W. Anderson, Phys. Rev. 109, 1492 (1958).

[30] I. M. Lifshits, Sov. Phys. JETP 17, 1159 (1963).

[31] P. A. Lee and T. V. Ramakrishnan, Rev. Mod. Phys. 57, 287 (1985).

[32] P. Phillips, Ann. Rev. Phys. Chem. 44, 115 (1993).

[33] I. M. Lifshits, S. A. Gredeskul, and L. A. Pastur, Introduction to the Theory of Disordered Systems (Wiley, New York, 1987).

[34] R. E. Borland, Proc. R. Soc. London Ser. A 274, 529 (1963).

[35] F. Laruelle and B. Etienne, Phys. Rev. B 37, 4816 (1988).

[36] K. Hirose, D. Y. K. Ko, and H. Kamimura, J. Phys. Condens. Matter 4,

[37] D. B. Laks, S.-H. Wei, and A. Zunger, Phys. Rev. Lett. 69, 3766 (1992).

[38] E. G. Wang, J. H. Xu, W. P. Su, and C. S. Ting, Appl. Phys. Lett. 63, 1411 (1993).

[39] E. G. Wang, J. H. Xu, W. P. Su, and C. S. Ting, Appl. Phys. Lett. 64, 443

[40] E. G. Wang, W. P. Su, and C. S. Ting, J. Appl. Phys. 76, 3664 (1994).

[41] V. Kumar and G. Ananthakrishna, Phys. Rev. Lett. 59, 1476 (1987).

[42] X. Chen and S. Xiong, Phys. Rev. B 48, 5273 (1993).

[43] M. Kasu, T. Yamamoto, S. Noda, and A. Sasaki, Appl. Phys. Lett. 59, 800

[45] D. J. Arent, R. G. Alonso, G. S. Horner, D. Levi, M. Bode, A. Mascaren-

[46] T. Yamamoto, M. Kasu, S. Noda, and A. Sasaki, J. Appl. Phys. 68, 5318

[47] K. A. Mäder, L.-W. Wang, and A. Zunger, Phys. Rev. Lett. 74, 2555 (1995).

[48] K. A. Mäder and A. Zunger, Phys. Rev. B 50, 17 393 (1994).

[49] L.-W. Wang and A. Zunger, J. Chem. Phys. 100, 2394 (1994).

[50] B. Jonsson and S. T. Eng, IEEE J. Quantum Electron. QE-26, 2025 (1990).

[51] If the δ layers are arranged periodically in a host SL, R of Eq. (3) still bears the meaning of the "concentration" of δ layers, and $R \propto L^{-1}$, where L is the (fixed) distance between the δ layers.

[52] S.-H. Wei and A. Zunger, J. Appl. Phys. 63, 5794 (1988).

[53] D. M. Bylander and L. Kleinman, Phys. Rev. B34, 5280 (1986).

[54] W. Ge, W. D. Schmidt, M. D. Sturge, L. N. Pfeiffer, and K. W. West, J. Lumin. 59, 163 (1994).

[55] For $n=5$ and $n=6$ we find that the lowest conduction state at $\bar{Z}$ is ≤ 10 meV lower than $\Gamma(X_z)$, making these SLs indirect-gap materials (see Table III in Ref. 48); however, this energy difference is too small to allow a conclusive prediction on the pseudodirect/indirect nature of the band gap.

[58] S. B. Zhu, M. L. Cohen, S. G. Louie, D. Tomanek, and M. S. Hybertsen,

[59] K. A. Mäder and A. Zunger, Appl. Phys. Lett. 64, 2882 (1994).

[60] Z. Ikonic, G. P. Srivastava, and J. C. Inkson, Phys. Rev. B 46, 15 150 (1992).

[61] R. Cingolani, L. Tapfer, and K. Ploog, Appl. Phys. Lett. 56, 1233 (1990).

[62] See, for example, G. Baym, Lectures on Quantum Mechanics, 9th ed.

[63] K. A. Mäder and A. Baldereschi, Mater. Res. Soc. Symp. Proc. 240, 597

[65] M. Kasu, T. Yamamoto, S. Noda, and A. Sasaki, Jpn. J. Appl. Phys. 29,

[67] This discrepancy can be traced back to the EMA error in the $(GaAs)_n(AlAs)_n$, o-SL of $n \sim 1$, 2 in Fig. 7. Around $n \sim 1$, 2, the EMA $\bar{\Gamma}_c(\Gamma)$ (001) states have much larger energies than their EPM counterparts. Apparently, this difference retains in the d-SL.

for our computational unit cell as was used for the MBE growth of the po-SL.